Mathematical Model and Machining Method for Spiral Flute Rake Faces of Hourglass Worm Gear Hob

YANG Jie[1], *LI Haitao*[1,2*], *RUI Chengjie*[1], *HUANG Yi*[1], *ZHANG Xiaodi*[3]

1. College of Engineering, China Agricultural University, Beijing 100083, P. R. China;
2. Key Laboratory of Optimal Design of Modern Agricultural Equipment in Beijing, China Agricultural University, Beijing 100083, P. R. China;
3. Beijing Kuiente Technology Co, Ltd, Beijing 100043, P. R. China

(Received 11 December 2017; revised 2 April 2018; accepted 27 April 2019)

Abstract: To improve the cutting performance of an hourglass worm gear hob and the accuracy of the resulting worm gear, the rake angles of the teeth on the pitch circle should be reduced. A method of forming the spiral flutes by using a variable transmission ratio was developed. This method ensures that the rake angles on the indexing torus of each tooth are approximately 0°. Based on the gear meshing theory and the hourglass worm forming method, the discretization mathematical model of the rake face of a planar double-enveloping worm gear hob was established by using cylindrical generating surface, and the feed parameters for machining the rake face for a variable transmission ratio were obtained. The spiral flute was simulated and the hob was machined on a four-axis CNC milling machine. A contourgraph was used to measure the rake angle. The measurement results showed that the proposed method can reduce the absolute value of the rake angle on both sides of the cutting teeth, which can be used for machining the spiral flute rake face of an hourglass worm gear hob.

Key words: hourglass worm gear hob; cylindrical generating surface; spiral flute; rake face; rake angle

CLC number: TH132.4 **Document code**: A **Article ID**: 1005-1120(2019)03-0401-12

0 Introduction

Compared with cylindrical worm gear drives, hourglass worm gear drives are smaller and has a greater load capacity, and higher transmission efficiency[1-3]. The accuracy of the worm gear tooth surfaces depends on the performance of the worm gear hob used to machine the worm gear[4-5]. Chang et al.[6] developed a general mathematical model for gears manufactured with computer numberical control (CNC) hobbing machines. Geometry errors in hob cutters are one of the most important factors influencing the quality of the machined gears. Liston[7] investigated gear geometry errors due to sharpening errors in the hob cutter. Winter and Wilkesmann[8], Simon[9], Bosch[10] and Bär[11] proposed various methods of obtaining more accurate worm gear surfaces. Kin[12] studied the variations in worm gear tooth surfaces due to deviations in the cutting edges of hob cutters. To the knowledge of the authors, investigation into the milling profiles of hob cutters with helix gashes has not been addressed.

The type of flutes on the hob affects the shape of the cutting edge and determines the rake angles on both sides of the cutting teeth, which affects the accuracy of the worm gear that the hob produces and the machining efficiency. With straight flutes, one side of the cutting teeth has a positive rake angle and the other has a negative rake angle. Large negative rake angles can cause problems in machining. These factors reduce the worm gear tooth surface accuracy. Large positive rake angles result in faster

*Corresponding author, E-mail address: h.li@cau.edu.cn.

How to cite this article: YANG Jie, LI Haitao, RUI Chengjie, et al. Mathematical Model and Machining Method for Spiral Flute Rake Faces of Hourglass Worm Gear Hob[J]. Transactions of Nanjing University of Aeronautics and Astronautics, 2019,36(3):401-412.
http://dx.doi.org/10.16356/j.1005-1120.2019.03.004

tooth wear, i.e., a reduced service life of the hob. Therefore, the hob is usually designed with spiral flutes shaped to ensure that the rake angles on both sides of the teeth are approximately zero.

Dong[13] and Liu[14] developed a mathematical model for worm gear hobs with straight flutes. If the spiral angles are small, straight flutes are used because the resulting negative rake angles on one side of the cutting teeth do not significantly affect cutting. However, spiral flutes are used for hobs with multiple threads because with straight flutes, the magnitudes of the negative rake angles on one side of the cutting teeth are sufficiently large that the cutting edges are not effective[15-19]. Chang[20] developed a general mathematical model of the helix gash of a hob cutter and studied the errors between the actual machined surface and the mathematical rake surface that are caused by the movement of the cylindrical surface. Liu et al.[21] analyzed the orthogonal curve of the spiral line of Hindley worm gears. The transmission ratio of the orthogonal curve of the worm gear was derived, but a mathematical expression for this orthogonal curve was not provided. Liu[22] studied the forming of the spiral flutes in gear hobs using a grinding process. It is difficult to determine the geometry of the spiral flutes in worm gear hobs because the shape and angle of the cutting edges on an hourglass worm gear hob are different. Furthermore, it is difficult to ensure that the rake angles on the right and the left edges of the teeth are near zero[1,19].

In this paper, we propose a method for generating spiral flutes in an hourglass worm gear hob. An expression for the transmission ratio for generating the spiral flutes using a cylindrical generating surface is derived. The mathematical model of the spiral flute rack faces is obtained. The software VERICUT is used to simulate the machining of the spiral flutes of a hob. The rake angles on both sides of the teeth of the simulated workpiece are calculated, and these values are compared with those obtained from the equations to validate the mathematical model and the design method.

1 Mathematical Model of Spiral Flute Rake Faces

As shown in Fig.1, the plane Σ_d of the grinding wheel forms the spiral groove surface Σ_1 in a planar double-enveloping hourglass worm. The surface Σ_1 is the initial surface for a worm gear hob, which is used to cut a worm gear tooth surface, where the worm gear and a matching hourglass worm are a planar double-enveloping worm pairs. The spiral surface Σ_1 is referred to as the basic worm of the hob.

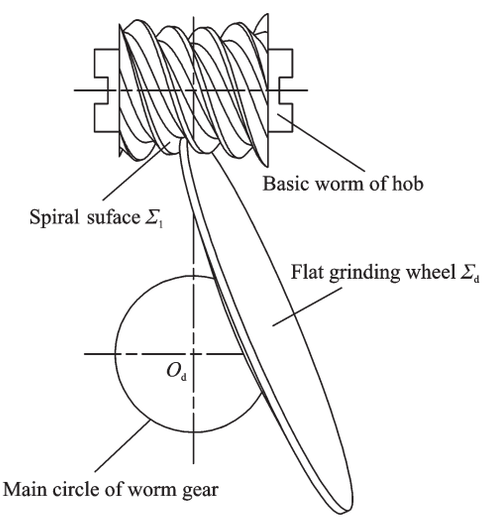

Fig.1 Forming the basic worm using a flat grinding wheel

As shown in Fig.2, a cylindrical surface Σ_{qd} is the envelope for forming the spiral flutes that are cut into the basic worm of the hob, creating the tooth rake faces Σ_2. The intersection lines of the spiral surface Σ_1 of the basic hob worm and the rake faces Σ_2

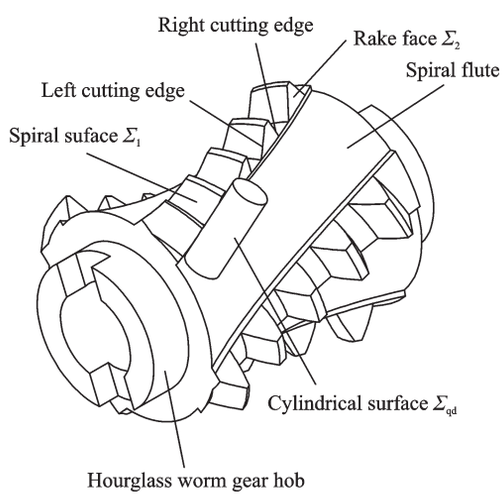

Fig.2 Forming the spiral flutes using a cylindrical surface

are created by cutting the spiral flutes form the cutting edges of the hob teeth. The method used to form the rake faces Σ_2 of the spiral flutes affects the geometry of the edges, which determines the rake angles on the left and the right sides of the cutting teeth. The machining efficiency and the accuracy of the worm gear depend on the rake angles of the teeth.

1.1 Coordinate systems for a plane Σ_d envelope of spiral surface Σ_1

It is assumed that the spiral surface of the basic hob worm is ground with a flat grinding wheel. A right-handed Cartesian coordinate system σ_1, as illustrated in Fig.3, is defined. Two static coordinate systems σ_{oi} (O_{oi}; $\boldsymbol{i}_{oi}$, $\boldsymbol{j}_{oi}$, $\boldsymbol{k}_{oi}$) (i=1, 2) are introduced, where the subscript "1" indicates the frame fixed to the worm and the subscript "2" indicates the frame fixed to the worm gear. The dimension a= $|O_1O_2|$ is the center distance between the worm and the worm gear.

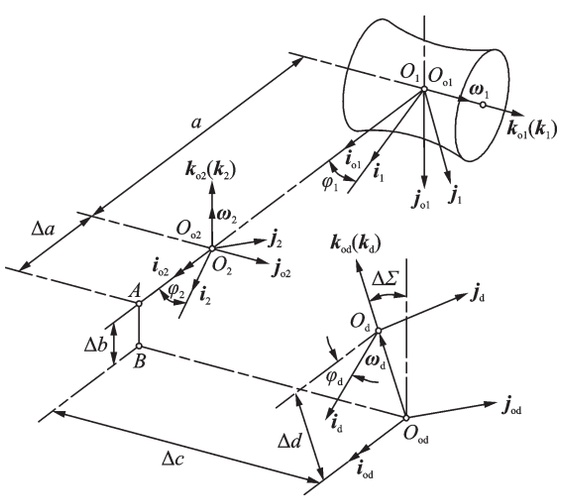

Fig.3 Coordinate systems of the basic hob worm and the grinding head

Two moving coordinate systems σ_i (O_i; $\boldsymbol{i}_i$, $\boldsymbol{j}_i$, $\boldsymbol{k}_i$) (i=1, 2) are defined, where subscript i means the same as defined above 1 is fixed to the worm and 2 is fixed to the worm gear. The instantaneous angular position of the worm is φ_1, the instantaneous angular position of the worm gear is φ_2= $i_{21}\varphi_1$, here i_{21} is the ratio of the worm and the worm gear. The initial positions of the worm and the worm gear are φ_1=φ_2=0°.

A static coordinate system σ_{od} (O_{od}; $\boldsymbol{i}_{od}$, $\boldsymbol{j}_{od}$, $\boldsymbol{k}_{od}$) is fixed to the base. A moving coordinate system σ_d (O_d; $\boldsymbol{i}_d$, $\boldsymbol{j}_d$, $\boldsymbol{k}_d$) is fixed to the grinding head holder. When grinding the spiral surface of the basic hob worm, the workpiece (i.e., worm blank) rotates with a speed $\boldsymbol{\omega}_1$ about the axis $\boldsymbol{k}_{o1}$, and the instantaneous angular position is φ_1=$|\boldsymbol{\omega}_1|\cdot\Delta t$. The rotational speed of the grinding head holder about the $\boldsymbol{k}_{od}$ axis is $\boldsymbol{\omega}_d$, the angular position is φ_d=$|\boldsymbol{\omega}_d|\cdot\Delta t$, and the initial positions of the worm blank and the grinding head holder are φ_1=φ_2=0°.

The instantaneous angular position φ_1 of the worm blank is proportional to the instantaneous angular position φ_d of the grinding head holder, that is, φ_1=$i_{1d}\varphi_d$, where i_{1d} is the speed ratio of the worm blank and the grinding head holder.

Worm drives produced with current methods do not mesh well. This problem can be addressed by modification. The worm surface can be modified by changing the relative position and motion of the grinding head holder and the worm blank. Specifically, the following relations should be satisfied: Δb= Δc= Δd=0, $\Delta\Sigma$=0, Δa>0, and Δi= $i_{1d}-i_{12}$, where Δa is the center distance correction, Δb the correction perpendicular to the axis of the worm, Δc the correction along the axis of the worm, Δd the displacement along the axis of the grinding head holder, $\Delta\Sigma$ the angle correction, Δi the transmission ratio correction, i_{1d} the speed ratio of the worm blank and the grinding head holder, and i_{12} the transmission ratio of the worm pair[1].

The equations describing the spiral surface of the basic hob worm in the coordinate system σ_1 are as follows

$$\begin{cases}(\boldsymbol{r}_1)_1=[x_1,y_1,z_1]^{\mathrm{T}}\\ \Phi_1=(\boldsymbol{v}_{d1})_1\cdot(\boldsymbol{n}_1)_1=0\end{cases}\tag{1}$$

where (x_1, y_1, z_1) is an arbitrary point on the spiral surface in the coordinate system σ_1; $(\boldsymbol{r}_1)_1$ the coordinates of a point; $(\boldsymbol{v}_{d1})_1$ the relative speed between a point on the cutting plane and a point on the basic hob worm; and $(\boldsymbol{n}_1)_1$ the unit normal vector of an arbitrary point on the spiral surface of the basic hob

worm[1,13-14].

1.2 Coordinate systems for cylindrical surface Σ_{qd} envelope of spiral flute rack face Σ_2

The rake faces of the hourglass worm gear hob are formed by cutting the spiral flutes. The flutes are cut using a cylindrical cutter. A right-handed Cartesian coordinate system is defined as illustrated in Fig.4. A static coordinate system σ_{qo1} (O_{qo1}; $\boldsymbol{i}_{qo1}$, $\boldsymbol{j}_{qo1}$, $\boldsymbol{k}_{qo1}$) is fixed to the base. A moving coordinate system σ_{q1} (O_{q1}; $\boldsymbol{i}_{q1}$, $\boldsymbol{j}_{q1}$, $\boldsymbol{k}_{q1}$) is fixed to the basic hob worm, where O_{qo1} is the origin of the coordinate system, O_{qo1} coincides with O_{q1}, and $\boldsymbol{k}_{qo1}=\boldsymbol{k}_{q1}$ coincides with the rotational axis of the basic hob worm.

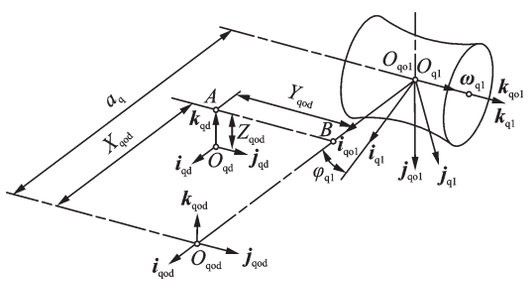

Fig.4 Coordinate systems for rake face machining

A static coordinate system σ_{qod} (O_{qod}; $\boldsymbol{i}_{qod}$, $\boldsymbol{j}_{qod}$, $\boldsymbol{k}_{qod}$) is fixed to the base, where $\boldsymbol{i}_{qod}=\boldsymbol{i}_{qo1}$ and $\boldsymbol{k}_{qod}=-\boldsymbol{j}_{qo1}$. A moving coordinate system σ_{qd} (O_{qd}; $\boldsymbol{i}_{qd}$, $\boldsymbol{j}_{qd}$, $\boldsymbol{k}_{qd}$) is fixed to the tool holder, where $\boldsymbol{i}_{qd}=\boldsymbol{i}_{qod}$, $\boldsymbol{k}_{qd}$ coincides with the tool holder axis. Z_{qod} denotes the distance from the tool holder axis O_{qd} to point A, and the dimension $a_q=|O_{qod}O_{qo1}|$ is the distance between the origins of the two coordinate systems. The point O_{qod} and the rotational axis of the basic hob worm lie in the plane S.

The instantaneous velocities of the tool holder in the $\boldsymbol{i}_{qod}$ and $\boldsymbol{j}_{qod}$ axes are $\boldsymbol{v}_x$ and $\boldsymbol{v}_y$, respectively, and the displacements are $X_{qod}=\int_0^t|\boldsymbol{v}_x|\mathrm{d}t+X_{qod}(0)$, $Y_{qod}=\int_0^t|\boldsymbol{v}_y|\mathrm{d}t+Y_{qod}(0)$, respectively, where the displacements satisfy the relation $X_{qod}=\sqrt{r_2^2-Y_{qod}^2}$. The changes in the displacement along the two axes are $\mathrm{d}X_{qod}=|\boldsymbol{v}_x|\mathrm{d}t$ and $\mathrm{d}Y_{qod}=|\boldsymbol{v}_y|\mathrm{d}t$.

The instantaneous rotational speed of the basic hob worm about the $\boldsymbol{k}_{qo1}$ axis is $\boldsymbol{\omega}_{q1}$, the angular position of the hob worm is $\varphi_{q1}=\int_0^t|\boldsymbol{\omega}_{q1}|\mathrm{d}t+\varphi_{q1}(0)$, and the change in the angular position is $\mathrm{d}\varphi_{q1}=|\boldsymbol{\omega}_{q1}|\mathrm{d}t$. The initial position is $Z_i=0$, $\varphi_{q1}(0)=\varphi_h$, $Y_{qod}(0)=0$, $X_{qod}(0)=r_2$, where φ_h is the angular position of the worm blank when the throat of the basic worm rotates into the plane S.

The instantaneous rotational speed $\boldsymbol{\omega}_{q1}$ of the basic hob worm about the $\boldsymbol{k}_{qo1}$ axis is proportional to the instantaneous velocity $\boldsymbol{v}_y$ of the tool holder along the $\boldsymbol{j}_{qod}$ axis, i.e.

$$\boldsymbol{\omega}_{q1}=i_{qd1}\cdot\boldsymbol{v}_y \tag{2}$$

where i_{qd1} is the ratio of the basic hob worm rotation and the cylindrical surface movement, which is referred to as the transmission ratio.

1.3 Transmission ratio i_{qd1}

The variable transmission ratio i_{qd1} is obtained as follows[23-26]

$$i_{qd1}=-\frac{r_2^2}{i_{1d}\cdot(a-\sqrt{r_2^2-Z_i^2})\cdot\sqrt{r_2^2-Z_i^2}}\cdot\frac{1}{[a-r_2\cdot\cos(\varphi_d-\alpha)]} \tag{3}$$

If $Z_i=0$, $\varphi_d=\alpha$; thus, the transmission ratio is fixed and can be obtained as follows

$$i_{qd1}=-\frac{r_2}{i_{1d}\cdot(a-r_2)^2} \tag{4}$$

1.4 Geometry and normal vector of cylindrical cutter

Fig.5 shows the cylindrical surface that generates the spiral flutes. The equation of the cylinder Σ_{qd} in the moving coordinate system σ_{qd} is

$$(\boldsymbol{r}_{qd})_{qd}=[x_{qd},y_{qd},z_{qd}]^{\mathrm{T}}=[h,r_x\cos\theta,r_x\sin\theta]^{\mathrm{T}} \tag{5}$$

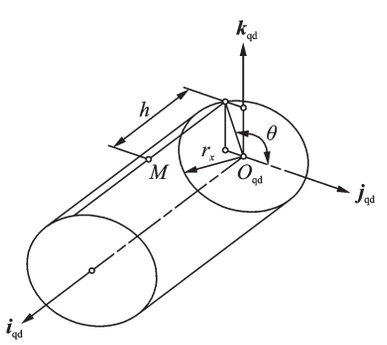

Fig.5 Cylindrical generating surface

The equation of the cylinder Σ_{qd} in the static coordinate system σ_{qod} is

$$(\boldsymbol{r}_{qd})_{qod}=(\boldsymbol{r}_{qd})_{qd}+(\boldsymbol{O}_{qod}\boldsymbol{O}_{qd})_{qod} \tag{6}$$

where the position of $\boldsymbol{O}_{qd}$ relative to $\boldsymbol{O}_{qod}$ is determined as follows

$$(\boldsymbol{O}_{qod}\boldsymbol{O}_{qd})_{qod}=(\boldsymbol{O}_{qod}\boldsymbol{B})_{qod}+(\boldsymbol{BA})_{qod}+(\boldsymbol{AO}_{qd})_{qod}=X_{qod}\boldsymbol{i}_{qod}+Y_{qod}\boldsymbol{j}_{qod}+Z_{qod}\boldsymbol{k}_{qod}=[X_{qod},Y_{qod},Z_{qod}]^{T} \tag{7}$$

The equation of the cylinder Σ_{qd} in the static coordinate system σ_{q1} is

$$(\boldsymbol{r}_{qd})_{q1}=\boldsymbol{R}[\boldsymbol{k}_{q1},-\varphi_{q1}]\{\boldsymbol{R}[\boldsymbol{i}_{qo1},90°][(\boldsymbol{r}_{qd})_{qod}+(\boldsymbol{O}_{qo1}\boldsymbol{O}_{qod})_{qo1}]\} \tag{8}$$

where $(\boldsymbol{O}_{qo1}\boldsymbol{O}_{qod})_{qo1}$ is the distance between the origins of the two coordinate systems, i.e., $(\boldsymbol{O}_{qo1}\boldsymbol{O}_{qod})_{qo1}=a_q$.

The position of an arbitrary point on the rake face in the coordinate system σ_{q1} is

$$(\boldsymbol{r}_{q1})_{q1}=(\boldsymbol{r}_{qd})_{q1}=[x_{q1},y_{q1},z_{q1}]^{T} \tag{9}$$

where r_x is the radius of the cylindrical cutter and the parameters of the cylindrical generating surface are θ and h, which are both positive, i.e., $\theta\geqslant 0$ and $h\geqslant 0$.

The unit normal vector of the cylindrical generating surface is $(\boldsymbol{n}_{qd})_{qd}$ in the σ_{qd} coordinate system and $(\boldsymbol{n}_{qd})_{q1}$ in the σ_{q1} coordinate system. Eq.(11) shows the relation between $(\boldsymbol{n}_{qd})_{qd}$ and $(\boldsymbol{n}_{qd})_{q1}$ through a coordinate transformation

$$(\boldsymbol{n}_{qd})_{qd}=[0,-\cos\theta,-\sin\theta]^{T} \tag{10}$$

$$(\boldsymbol{n}_{qd})_{q1}=\boldsymbol{R}[\boldsymbol{k}_{q1},-\varphi_{q1}]\{\boldsymbol{R}[\boldsymbol{i}_{qo1},90°](\boldsymbol{n}_{qd})_{qd}\} \tag{11}$$

The orientation of $(\boldsymbol{n}_{qd})_{qd}$ is outward from the rake face.

In the σ_{q1} coordinate system, $(\boldsymbol{n}_{q1})_{q1}$ is the unit normal vector of an arbitrary point on the rake face, where

$$(\boldsymbol{n}_{q1})_{q1}=(\boldsymbol{n}_{qd})_{q1} \tag{12}$$

The expression for the unit normal vector of an arbitrary point on a rake face in the coordinate system σ_{qod} is

$$(\boldsymbol{n}_{q1})_{qod}=\boldsymbol{R}[\boldsymbol{i}_{qod},-90°](\boldsymbol{n}_{q1})_{q1} \tag{13}$$

1.5 Conjugate equation of the first envelope

In the σ_{qod} coordinate system, at the contact point, the relative speed between the cylindrical generating surface and the rake face is $(\boldsymbol{V}_{qd1})_{qod}$. The conjugate equation of the first envelope is obtained from gear theory[23-26].

$$\Phi_{qod}=(\boldsymbol{V}_{qd1})_{qod}\cdot(\boldsymbol{n}_{q1})_{qod}=0 \tag{14}$$

where

$$(\boldsymbol{V}_{qd1})_{qod}=(\boldsymbol{\omega}_{qd1})_{qod}\times(\boldsymbol{r}_{qd})_{qod}+(\boldsymbol{\omega}_{q1})_{qod}\times(\boldsymbol{O}_{qod}\boldsymbol{O}_{qo1})_{qod}+(\boldsymbol{v}_{qd1})_{qod} \tag{15}$$

$$(\boldsymbol{O}_{qod}\boldsymbol{O}_{qo1})_{qod}=a_q(-\boldsymbol{i}_{qod})=-a_q\boldsymbol{i}_{qod}=[-a_q,0,0]^{T} \tag{16}$$

The rotational speed of the basic hob worm in the σ_{q1} coordinate system is $(\boldsymbol{\omega}_{q1})_{q1}$, which can be expressed as

$$(\boldsymbol{\omega}_{q1})_{q1}=\frac{\mathrm{d}\varphi_{q1}}{\mathrm{d}t}\boldsymbol{k}_{q1}=\left[0,0,\frac{\mathrm{d}\varphi_{q1}}{\mathrm{d}t}\right]^{T} \tag{17}$$

The rotational speed of the basic hob worm in the σ_{qo1} coordinate system is $(\boldsymbol{\omega}_{q1})_{qo1}$, which can be expressed as

$$(\boldsymbol{\omega}_{q1})_{qo1}=\boldsymbol{R}[\boldsymbol{k}_{qo1},\varphi_{q1}](\boldsymbol{\omega}_{q1})_{q1}=\left[0,0,\frac{\mathrm{d}\varphi_{q1}}{\mathrm{d}t}\right]^{T} \tag{18}$$

The rotational speed of the basic hob worm in the σ_{qod} coordinate system is $(\boldsymbol{\omega}_{q1})_{qod}$, which can be expressed as

$$(\boldsymbol{\omega}_{q1})_{qod}=\boldsymbol{R}[\boldsymbol{i}_{qo1},-90°](\boldsymbol{\omega}_{q1})_{qo1}=\left[0,\frac{\mathrm{d}\varphi_{q1}}{\mathrm{d}t},0\right]^{T} \tag{19}$$

The relative rotational speed of the basic hob worm and the cylindrical surface in the σ_{qod} coordinate system is $(\boldsymbol{\omega}_{qd1})_{qod}$, which can be expressed as

$$(\boldsymbol{\omega}_{qd1})_{qod}=(\boldsymbol{\omega}_{qd})_{qod}-(\boldsymbol{\omega}_{q1})_{qod} \tag{20}$$

The cylindrical surface does not rotate, thus the rotational speed of the cutter $(\boldsymbol{\omega}_{qd})_{qod}$ is zero.

Substituting Eq.(19) and $(\boldsymbol{\omega}_{qd})_{qod}=0$ into Eq.(20), the relative rotational speed is obtained

$$(\boldsymbol{\omega}_{qd1})_{qod}=-(\boldsymbol{\omega}_{q1})_{qod}=\left[0,-\frac{\mathrm{d}\varphi_{q1}}{\mathrm{d}t},0\right]^{T} \tag{21}$$

The relative linear velocity of the basic hob worm and the cylindrical surface in the σ_{qod} coordinate system is $(\boldsymbol{v}_{qd1})_{qod}$, which can be expressed as

$$(\boldsymbol{v}_{qd1})_{qod}=(\boldsymbol{v}_{qd})_{qod}-(\boldsymbol{v}_{q1})_{qod} \tag{22}$$

The linear velocity of the cylindrical surface in the σ_{qod} coordinate system is $(\boldsymbol{v}_{qd})_{qod}$, which can be expressed as

$$(\boldsymbol{v}_{\mathrm{qd}})_{\mathrm{qod}}=\frac{\mathrm{d}X_{\mathrm{qod}}}{\mathrm{d}t}\boldsymbol{i}_{\mathrm{qod}}+\frac{\mathrm{d}Y_{\mathrm{qod}}}{\mathrm{d}t}\boldsymbol{j}_{\mathrm{qod}}=\left[\frac{\mathrm{d}X_{\mathrm{qod}}}{\mathrm{d}t},\frac{\mathrm{d}Y_{\mathrm{qod}}}{\mathrm{d}t},0\right]^{\mathrm{T}} \tag{23}$$

The basic hob worm has no translational motion, thus the linear velocity $(\boldsymbol{v}_{\mathrm{q1}})_{\mathrm{qod}}$ is zero.

Substituting Eq.(23) and $(\boldsymbol{v}_{\mathrm{q1}})_{\mathrm{qod}}=0$ into Eq.(22), the relative linear velocity is obtained

$$(\boldsymbol{v}_{\mathrm{qd1}})_{\mathrm{qod}}=\left[\frac{\mathrm{d}X_{\mathrm{qod}}}{\mathrm{d}t},\frac{\mathrm{d}Y_{\mathrm{qod}}}{\mathrm{d}t},0\right]^{\mathrm{T}} \tag{24}$$

Substituting Eqs.(6), (16), (19), (21), and (24) into Eq.(15), the relative speed between the cylindrical generating surface and the rake face is obtained

$$(\boldsymbol{V}_{\mathrm{qd1}})_{\mathrm{qod}}=\begin{bmatrix}\dfrac{\mathrm{d}X_{\mathrm{qod}}}{\mathrm{d}t}-\dfrac{\mathrm{d}\varphi_{\mathrm{q1}}}{\mathrm{d}t}\left(r_x\sin\theta+Z_{\mathrm{qod}}\right)\\ \dfrac{\mathrm{d}Y_{\mathrm{qod}}}{\mathrm{d}t}\\ \dfrac{\mathrm{d}\varphi_{\mathrm{q1}}}{\mathrm{d}t}\left(h+X_{\mathrm{qod}}\right)+\dfrac{\mathrm{d}\varphi_{\mathrm{q1}}}{\mathrm{d}t}a_{\mathrm{q}}\end{bmatrix}^{\mathrm{T}} \tag{25}$$

Substituting Eqs.(13) and (25) into Eq.(14), the following expression is obtained

$$\frac{\mathrm{d}Y_{\mathrm{qod}}}{\mathrm{d}t}\cdot(-\cos\theta)+\left[\frac{\mathrm{d}\varphi_{\mathrm{q1}}}{\mathrm{d}t}(h+X_{\mathrm{qod}})+\frac{\mathrm{d}\varphi_{\mathrm{q1}}}{\mathrm{d}t}a_{\mathrm{q}}\right]\cdot(-\sin\theta)=0 \tag{26}$$

Substituting Eq.(2) into Eq.(26), the following expression is obtained

$$\frac{\boldsymbol{v}_y}{\boldsymbol{\omega}_{\mathrm{q1}}}=-(h+X_{\mathrm{qod}}+a_{\mathrm{q}})\cdot\tan\theta \tag{27}$$

The conjugate equation of the first envelope is

$$h=-X_{\mathrm{qod}}-a_{\mathrm{q}}-\frac{1}{i_{\mathrm{qd1}}\cdot\tan\theta} \tag{28}$$

1.6 Equation for rake face

Eqs.(9) and (28) can define the rake face

$$\begin{cases}(\boldsymbol{r}_{\mathrm{q1}})_{\mathrm{q1}}=[x_{\mathrm{q1}},y_{\mathrm{q1}},z_{\mathrm{q1}}]^{\mathrm{T}}\\ h=-X_{\mathrm{qod}}-a_{\mathrm{q}}-\dfrac{1}{i_{\mathrm{qd1}}\cdot\tan\theta}\end{cases} \tag{29}$$

The following expression is obtained from Eq.(2)

$$i_{\mathrm{qd1}}=\frac{\mathrm{d}\varphi_{\mathrm{q1}}}{\mathrm{d}Y_{\mathrm{qod}}} \tag{30}$$

Since $\boldsymbol{v}_y$ and $\boldsymbol{\omega}_{\mathrm{q1}}$ are unknown, $Y_{\mathrm{qod}}=\int_0^t|\boldsymbol{v}_y|\mathrm{d}t+Y_{\mathrm{qod}}(0)$ and $\varphi_{\mathrm{q1}}=\int_0^t|\boldsymbol{\omega}_{\mathrm{q1}}|\mathrm{d}t+\varphi_{\mathrm{q1}}(0)$ cannot be determined using the Newton-Leibniz formula. Thus, Y_{qod} is discretized to obtain the relative motion for machining the spiral flutes using a variable transmission ratio.

If Z_i is an integer, at the axial coordinate Z_i of the basic hob worm ($-0.5L_{\mathrm{w}}\leqslant Z_i\leqslant 0.5L_{\mathrm{w}}$), the following expression is obtained

$$i_{\mathrm{qd1}}(Z_i)=-\frac{r_2^2}{i_{1\mathrm{d}}\cdot(a-\sqrt{r_2^2-Z_i^2})\cdot\sqrt{r_2^2-Z_i^2}}\cdot\frac{1}{[a-r_2\cdot\cos(\varphi_{\mathrm{d}}-\alpha)]} \tag{31}$$

The equations describing the machine motion for cutting the spiral flutes using a variable transmission ratio are

$$i_{\mathrm{qd1}}(Z_i)=\frac{\varphi_{\mathrm{q1}}(Z_i)-\varphi_{\mathrm{q1}}(Z_i-1)}{Y_{\mathrm{qod}}(Z_i)-Y_{\mathrm{qod}}(Z_i-1)} \tag{32}$$

$$X_{\mathrm{qod}}(Z_i)=\sqrt{r_2^2-Y_{\mathrm{qod}}^2(Z_i)} \tag{33}$$

The equations describing the machine motion for cutting the spiral flutes using a fixed transmission ratio are

$$i_{\mathrm{qd1}}=-\frac{r_2}{i_{1\mathrm{d}}\cdot(a-r_2)^2}=\frac{\varphi_{\mathrm{q1}}-\varphi_{\mathrm{h}}}{Y_{\mathrm{qod}}} \tag{34}$$

$$X_{\mathrm{qod}}=\sqrt{r_2^2-Y_{\mathrm{qod}}^2} \tag{35}$$

2 Calculation and Analysis of Hob Rake Angle

From Eqs.(1) and (29), equations describing the edge geometry of the hob can be obtained. As shown in Fig.6, the normal vector on the rake face and on the spiral surface are obtained at an arbitrary point on the edges of the hob, and the rake angles[27] are obtained as follows

$$V_{\mathrm{q}}=\arccos[(\boldsymbol{n}_{\mathrm{q1}})_1\cdot(\boldsymbol{n}_1)_1]-90^\circ \tag{36}$$

where $W_{\mathrm{q}}=\arccos[(\boldsymbol{n}_{\mathrm{q1}})_1\cdot(\boldsymbol{n}_1)_1]$ is the angle between the normal vectors of the rake face and the spiral surface. The expression of $(\boldsymbol{n}_{\mathrm{q1}})_1$, $(\boldsymbol{n}_1)_1$ and $(\boldsymbol{n}_{\mathrm{d}})_{\mathrm{d}}$ are as follows

$$(\boldsymbol{n}_{\mathrm{q1}})_1=\boldsymbol{R}[\boldsymbol{k}_{\mathrm{q1}},-\varphi_{\mathrm{q1}}]\{\boldsymbol{R}[\boldsymbol{i}_{\mathrm{qo1}},90^\circ](\boldsymbol{n}_{\mathrm{qd}})_{\mathrm{qd}}\} \tag{37}$$

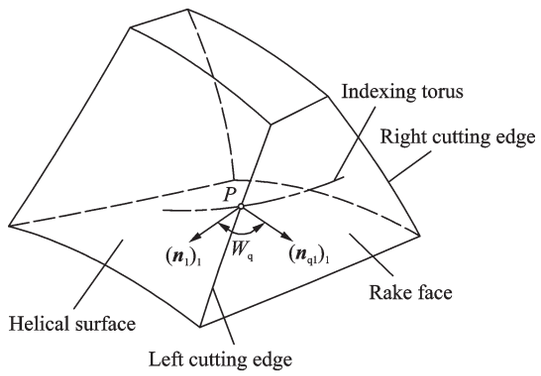

Fig.6 Angle between tooth surfaces at a point on tooth cutting edge

$$(\boldsymbol{n}_1)_1 = \boldsymbol{R}[\boldsymbol{k}_1, -\varphi_1]\{\boldsymbol{R}[\boldsymbol{i}_{o1}, 90°]\boldsymbol{R}[\boldsymbol{k}_{od}, \varphi_d](\boldsymbol{n}_d)_d\} \tag{38}$$

$$(\boldsymbol{n}_d)_d = [0, \cos\beta, \sin\beta]^T \tag{39}$$

The angles were calculated for an example hob, where the parameters for the example are given in Table 1. The rake angle of each tooth on the pitch circle was obtained for both fixed and variable transmission ratios. The rake angle results are shown in Tables 2, 3.

Table 1 Parameters for an example planar double-enveloping hourglass worm gear hob

No.	Parameter	Value
1	Center distance a/mm	160
2	Worm teeth z_1	4
3	Worm gear teeth z_2	40
4	Working length of worm gear hob L_w/mm	90
5	Diameter of main base circle d_b/mm	95
6	Inclination of plane grinding wheel β/(°)	22.5
7	Throat lead angle of worm on the pitch circle γ_m/(°)	21.420 5
8	Pressure angle on the pitch circle α/(°)	21.866 7
9	Worm radius of dedendum circle arc R_{f1}/mm	133.24
10	Worm radius of addendum circle arc R_{a1}/mm	122.24
11	Worm gear pitch diameter d_2/mm	255
12	Worm pitch diameter d_1/mm	65
13	Transverse module m_t	6.38
14	Tooth thickness of worm on the pitch circle arc s_1/mm	9.41

Table 2 Hob tooth rake angles on the pitch circle obtained using a fixed transmission ratio

Edge location	Tooth				
	No.1	No.2	No.3	No.4	No.5
Left side	1.708 83	−0.060 04	−0.501 66	1.129 17	4.830 84
Z_i	−38.171 39	−21.520 36	−4.226 86	13.246 70	30.652 93
Right side	−5.341 03	−1.637 29	−0.085 59	−0.667 29	−2.642 67
Z_i	−30.950 36	−13.517 04	3.920 86	21.148 44	37.881 56

Table 3 Hob tooth rake angles on the pitch circle obtained using a variable transmission ratio

Edge location	Tooth				
	No.1	No.2	No.3	No.4	No.5
Left side	0.445 06	0.067 97	−0.036 67	0.131 01	0.411 12
Z_i	−38	−21	−4	13	31
Right side	−0.378 63	−0.116 36	0.087 35	−0.062 32	−0.511 75
Z_i	−31	−13	4	21	38

The rake angles on the pitch circle obtained using a fixed transmission ratio and a variable transmission ratio are plotted in Fig.7.

(1) As shown in Table 2, when the spiral flutes are machined using a fixed transmission ratio, the left- and the right-side rake angles of the hob teeth vary between ±5.4°. The rake angles on the right side are negative. As shown in Fig.7, the absolute values of the rake angles from the exit (position $Z_i = -0.5L_w$) to the inlet (position $Z_i = 0.5L_w$) of

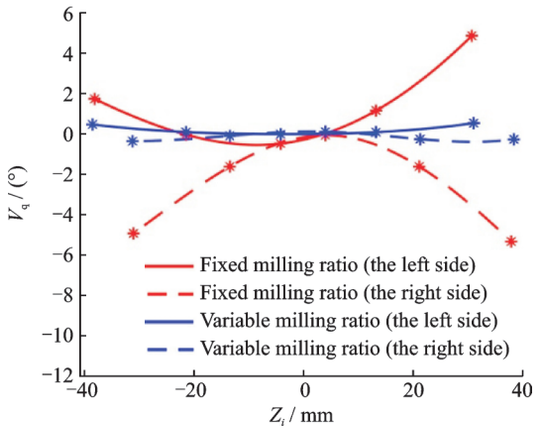

Fig.7 Hob tooth rake angle vs. axial position for fixed and variable transmission ratios

the hob initially decrease but then increase. The magnitudes of the rake angles on the throat teeth are minimal.

(2) As shown in Table 3, when the spiral flutes are machined using a variable transmission ratio, the left- and the right-side rake angles of the hob are between ±0.52°. Compared with fixed transmission ratio, use variable transmission ratio to form the spiral flutes, the rake angles on both sides of the hob tooth are much smaller. As shown in Fig.7, the right- and left-side rake angles are both approximately zero. The cutting performance on both sides of the teeth will be significantly improved.

3 Simulation of Spiral Flute Forming

The machining of the example hob with four threads, shown in Table 1, was simulated using the software VERICUT. In the simulation, a four-axis CNC machine with a B axis, a C axis, an X axis, and a Z axis was assumed[28-29].

The simulation parameters for the first spiral flute are shown in Table 4. The parameters for the X and Z axes were held constant, and the parameters for the C axis were given as 90°, 180°, 270° to generate the second, the third, and the fourth spiral flutes, respectively.

The simulated machined surfaces of the basic hob worm and the final hob with spiral flutes are shown in Fig.8.

Table 4 Machine motion parameters for machining spiral flutes using a variable transmission ratio

No.	C-axis/(°)	X-axis/mm	Z-axis/mm
1	210.823	117.287	−50
2	211.258 3	117.708 3	−49
3	211.700 7	118.119 6	−48
4	212.150 2	118.521 1	−47
5	212.607	118.912 8	−46
⋮	⋮	⋮	⋮
97	268.150	118.912 8	46
98	268.607	118.521 1	47
99	269.057	118.119 6	48
100	269.499	117.708 3	49
101	269.934	117.287	50

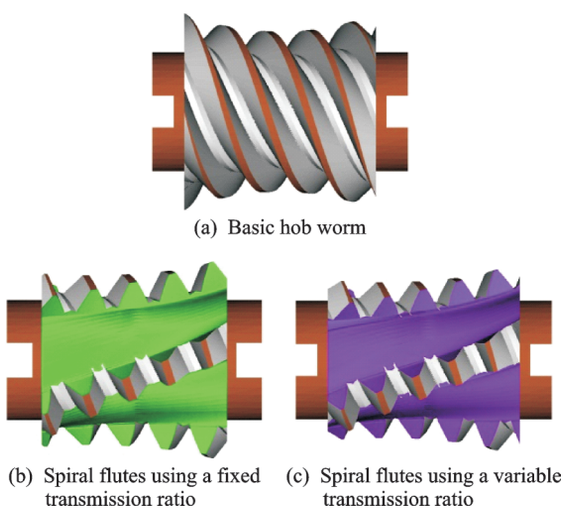

(a) Basic hob worm

(b) Spiral flutes using a fixed transmission ratio

(c) Spiral flutes using a variable transmission ratio

Fig.8 Simulation results

The geometry of the final hob surface was used to obtain the angle W_q between the normal vectors of the rake face and the spiral surface, as show in Fig.9. The rake angle V_q on both sides of the teeth was obtained using the formula $V_q = W_q - 90°$, and the results are shown in Table 5.

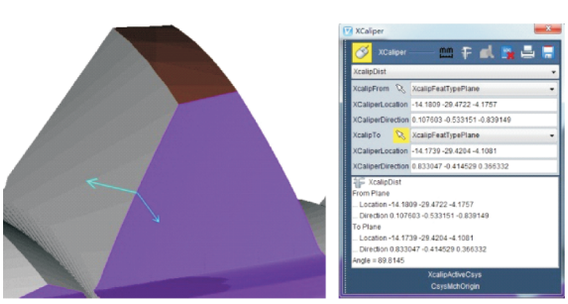

(a) Normal vectors of rake face and spiral surface

(b) Example of angle calculations

Fig.9 Angles of the final tooth surfaces

Table 5 Rake angles on pitch circle for teeth machined with a variable transmission ratio

Edge location	Tooth				
	No.1	No.2	No.3	No.4	No.5
Left side	0.110 1	0.190 9	−0.185 5	0.217 2	0.156 3
Z_i	−38.532 1	−21.471 7	−4.108 1	13.192 9	31.045 2
Right side	−0.252 4	−0.220 6	0.174 1	−0.315 6	−0.192 2
Z_i	−31.272 5	−13.504 5	4.127 4	21.269 0	38.384 9

The measurement results in Table 5 show that the method can reduce the absolute value of the rake angles on both sides of the hob, and the rake angles are between −0.4° and 0.3°.

4 Experiments and Measurements

The hob machining experiment was conducted on a CNC milling machine with A, X, Y, Z four-axis linkage. The model of the machine tool was Beijing Jingdiao JDVT700T-A13S. The A-axis of the machine tool was the rotational movement axis, and the X, Y, and Z axes were the linear movement axes. The parameters of the experimental hob were the same as Table 1. The hourglass worm gear hob machining experiment is shown in Fig.10.

(a) Hob machining process

(b) Spiral flutes worm gear hob

Fig.10 Hourglass worm gear hob machining experiment

One row of teeth on the hourglass worm gear hob was cut and number of teeth was counted after cutting, as shown in Fig.11.

The rake angle of each tooth was measured using an S neox contourgraph. The measurement accuracy of optical profiler was 0.1 μm. The Nikon DI

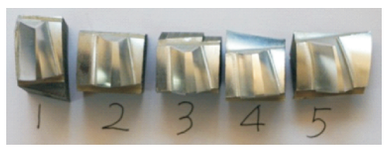

Fig.11 Single tooth and its number

20X objective was used, the scanning area resolution was 1 360 px×1 024 px, and the scanning range was T=10 μm, B=30 μm. In the "Confocal" mode, contour data were collected on the measured point on the cutting edge and the measured data was saved as "*.plux" file using the SensoSCAN menu. The data acquisition process is shown in Fig.12.

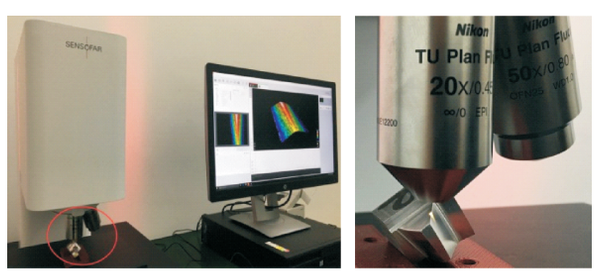

Fig.12 Collect data of the point being measured

We loaded the "*.plux" file data measured by Sneox into SensoPRO to analyze the measurement. As shown in Fig.13(a), the measurement data of the rake face and the spiral face and the cutting edge of the cutting teeth were imported into SensoPRO. As shown in Fig.13(b), the cutting edge was rotated to a vertical position for easy measurement. As shown in Fig.13(c), two planes near the cutting edge were selected and the angle between the two planes were measured. The results of the measurements are shown in Table 6.

It can be seen from Table 6 that the absolute value of the rake angles on both sides of each tooth is small, and the maximum is the right side rake angle of the tooth No.1, the value is −0.409 7°, and

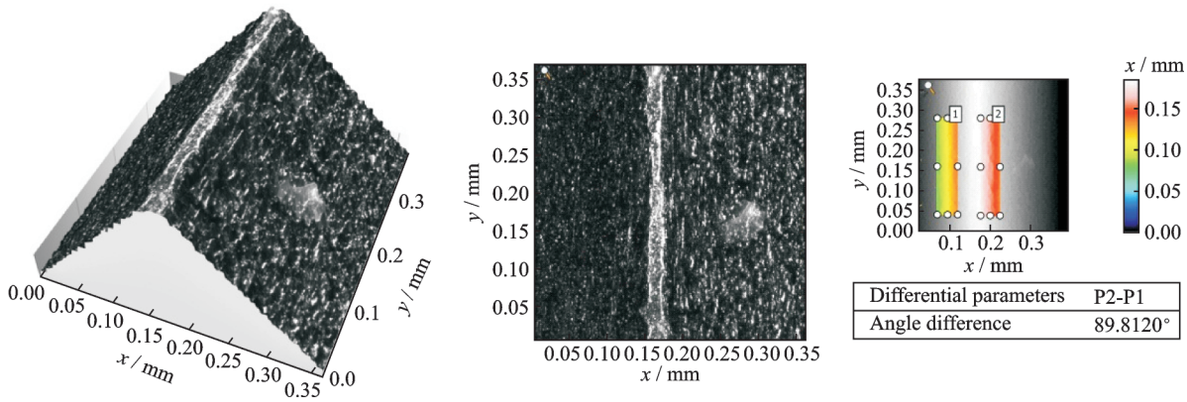

(a) Importing measured data (b) Adjusting position of the cutting edge (c) Selecting two planes

Fig.13 Analysis and measurement of angles

Table 6 Rake angles measured by contourgraph

Edge location	Tooth				
	No.1	No.2	No.3	No.4	No.5
Left side	0.277 4	−0.188 0	−0.305 2	0.393 3	−0.084 8
Right side	−0.409 7	0.125 3	0.300 6	−0.187 2	−0.331 6

the minimum is the left side rake angle of the tooth No.5, which is −0.084 8°. Compared with Table 3, the measurement results are biased. The maximum error is the left side rake angle of the tooth No.5, which is 0.495 92°; and the minimum error is the right side rake angle of the tooth No.1, which is 0.031 06°. The error is caused by the selected position of the two measurement planes.

5 Conclusions

(1) A method for machining spiral flutes in an hourglass worm gear hob is presented, and equations describing the spiral flutes rack face are obtained. The transmission ratio between the tool holder and the hob workpiece is derived. The correctness of the mathematical model is verified using a simulation of the machining process. The equations developed can provide a reference for the design and machining of the flutes in hourglass worm gear hobs.

(2) The required machine tool motions for machining the spiral flutes are obtained. The displacement of a cylindrical generating surface along the basic hob worm is discretized to enable the computation of the motion parameters. The rake angles of the resulting hob teeth are calculated. In addition, the rake angles of the teeth obtained using a variable transmission ratio and a fixed transmission ratio are analyzed.

(3) The hob machining experiment is conducted. The contourgraph is used to measure the rake angle of the hob. The measurement results show that the rake angles on both sides of the teeth are between −0.409 7° and 0.393 3°. The measurement results verify the correctness of the mathematical model and the feasibility of this processing method.

References

[1] DONG Xuezhu. Design and modification of enveloping worm gearing[M]. Beijing: China Mechanical Industry Press, 2004. (in Chinese)

[2] PAVLOV A. Method of globoid worm thread and worm wheel teeth: US3875635 [P]. 1975-04-15.

[3] TAKAO S, MINORU M. Globoid worm gear generating method: US4184795 [P]. 1980-02-22.

[4] TANG Jiansheng. Cutting and cutting tools[M]. Wuhan: China Wuhan University of Technology Press, 2009. (in Chinese)

[5] SIMON V. Hob for worm gear manufacturing with circular profile[J]. International Journal of Machine Tools and Manufacture, 1993, 33(4): 615-625.

[6] CHANG S L, TSAY C B, NAGATA S. A general mathematical model for gears generated by CNC hobbing machine[J]. ASME Journal of Mechanical Design, 1997, 119: 108-113.

[7] LISTON K. Hob basics: Part II[J]. Gear Technology, 1993, 10(6): 18-23.

[8] WINTER H, WILKESMANN H. Calculation of cylindrical worm gear drives of different tooth profiles [J]. ASME Journal of Mechanical Design, 1981, 103: 73-82.

[9] SIMON V. Grinding wheel profile for hob relief grinding[J]. ASME Journal of Mechanical Design, 1982, 104: 731-742.

[10] BOSCH M. Economical production of high precision gear worms and other thread shaped profiles by means of CNC-controlled worm and thread grinding machines [J]. Drive System Technique, 1988: 3-19.

[11] BARÄ G. CAD of worms and their machining tools[J]. Computers and Graphics, 1990, 14(3): 405-411.

[12] KIN V. Topological tolerancing of worm-gear tooth surfaces[J]. American Gear Manufactures Association, 1993: 1-6.

[13] DONG Liyang. Research on NC machining technology of enveloping worm gear hob[D]. Beijing: University of China Agricultural University, 2013. (in Chinese)

[14] LIU Guanyi. Research on CNC relief grinding technology of enveloping worm gear hob[D]. Beijing: University of China Agricultural University, 2016. (in Chinese)

[15] LITVIN F L, ALFONSO F. Gear geometry and applied theory[M]. Cambridge: Cambridge University Press, 2004.

[16] SIMON V. The influence of hob diameter on worm gear mesh[J]. Symposium on Machine Design, 1985, 4(2): 35-41.

[17] KANG S K, EHMANN K F, LIN C. A CAD approach to helical groove machining[J]. International Journal of Machine Tools and Manufacture, 1996, 36(1): 141-153.

[18] SHETH D S, MALKIN S. CAD/CAM for geometry and process analysis of helical groove machining[J]. Annals of the CIRP, 1990, 39(1): 129-132.

[19] ZHOU Liangyong. The modification principle and manufacturing technology of hourglass worm [M]. Changsha: China National University of Defense Technology Press, 2005. (in Chinese)

[20] CHANG S L. Helix gash of hob cutter manufactured by milling[J]. Journal of Materials Processing Technology, 2003, 142: 569-575.

[21] LIU Renxian, LIU Jiading. Study on curve of groove hob in circular waves[J]. Journal of Xi'an University of Architecture & Technology (Natural Science Edition), 1978(2): 95-101. (in Chinese)

[22] LIU Jiehua. Dressing calculation of the profile of the grinding wheel on the rake faces of the hob with zero rake angle[J]. Grinding Machine and Grinding, 1996(4): 25-26, 72. (in Chinese)

[23] LI Xiaozhen, GAO Zhu, WANG Xiaojun. Dynamic characteristics of modified face-gear drive system [J]. Journal of Nanjing University of Aeronautics and Astronautics, 2016, 48(6): 828-834. (in Chinese)

[24] LI Z M Q, WANG J, ZHU R P. Influence predictions of contact effects on mesh stiffness of face gear drives with spur gear[J]. Transactions of Nanjing University of Aeronautics and Astronautics, 2015, 32(5): 566-570.

[25] LITVIN F L. Theory of gearing[M]. USA: NASA Reference Publication, 1989.

[26] DONG Xuezhu. Gear meshing theory[M]. Beijing: China Machine Press, 1989. (in Chinese)

[27] JIANG Zhengjian, ZHANG Wei, LI Zhuyu. Calculation of the rake angle of micro drill and drilling test[J]. Journal of Dalian Institute of Light Industry, 2011, 30(2):145-147. (in Chinese)

[28] LI Yunlong, CAO Yan. NC machining simulation system VERICUT[M]. Xi'an: China Xi'an Jiao Tong University Press, 2005. (in Chinese)

[29] YANG Shengqun, TANG Xiumei. VERICUT NC machining simulation technology[M]. China Tsinghua University Press, 2010. (in Chinese)

Acknowledgements The work was supported by the National Natural Science Foundation of China (No. 51475460). We thank the State Key Laboratory of High Performance Complex Manufacturing of Central South University in China for the technical support using the VERICUT software.

Authors Mr. **YANG Jie** received the M.S. degree in Gansu Agricultural University in 2015. He is currently a doctoral candidate in China Agricultural University, majoring in mechanical design and theory. His research focuses on hourglass worm gear drive, including the design and manufacture of enveloping worm gearing and enveloping worm gear hob.

Dr. **LI Haitao** received the Ph.D. degree from China Agricultural University, Beijing, China, in 2009. From August 2009, he has been working at China Agricultural University,

Beijing. From October 2010, he has been working as a visiting scholar in the Brunel University in the United Kingdom AMEE, engaged in super-precision manufacturing. In May 2015, he joined the Key Laboratory of Optimal Design of Modern Agricultural Equipment in Beijing, China Agricultural University, Beijing.

Mr. **RUI Chengjie** received the M.S. degree in Tianjin University of Technology in 2014. He is currently a doctoral candidate in China Agricultural University, majoring in mechanical design and theory. His research focuses on hourglass worm gear drive, including the design and manufacture of enveloping worm gearing and enveloping worm gear hob.

Mr. **HUANG Yi** received the B.S. degree in China Agricultural University in 2017. He is currently a postgraduate student in China Agricultural University, majoring in mechanical engineering.

Ms. **ZHANG Xiaodi** has been working in Beijing Kuiente Technology Co, Ltd. Her research focuses on design and manufacture of hourglass worm gear reducer.

Author contributions Mr. **YANG Jie** designed the study, complied the models, conducted the analysis, interpreted the results and wrote the manuscript. Dr. **LI Haitao** directed the design of this paper, data analysis and paper writing. Mr. **RUI Chengjie** provided the idea of establishing mathematical model. Mr. **HUANG Yi** provided the methods of making pictures and drawing graphics. Ms. **ZHANG Xiaodi** provided the experimental ideas and conditions.

Competing interests The authors declare no competing interests.

(Production Editor: Xu Chengting)